JACS
JOURNAL OF THE AMERICAN CHEMICAL SOCIETY
Article
pubs.acs.org/JACS
Terms of Use CC-BY

Secondary Structure in the Core of Amyloid Fibrils Formed from Human β_2m and its Truncated Variant ΔN6

Yongchao Su,[†,⊥] Claire J. Sarell,[‡,⊥] Matthew T. Eddy,[†] Galia T. Debelouchina,[†,§] Loren B. Andreas,[†] Clare L. Pashley,[‡] Sheena E. Radford,[‡] and Robert G. Griffin*[,†]

[†]Department of Chemistry and Francis Bitter Magnet Laboratory, Massachusetts Institute of Technology Cambridge, Massachusetts 02139, United States

[‡]Astbury Centre for Structural Molecular Biology and School of Molecular and Cellular Biology, University of Leeds, Leeds LS2 9JT, United Kingdom

Supporting Information

ABSTRACT: Amyloid fibrils formed from initially soluble proteins with diverse sequences are associated with an array of human diseases. In the human disorder, dialysis-related amyloidosis (DRA), fibrils contain two major constituents, full-length human β_2-microglobulin (hβ_2m) and a truncation variant, ΔN6 which lacks the N-terminal six amino acids. These fibrils are assembled from initially natively folded proteins with an all antiparallel β-stranded structure. Here, backbone conformations of wild-type hβ_2m and ΔN6 in their amyloid forms have been determined using a combination of dilute isotopic labeling strategies and multidimensional magic angle spinning (MAS) NMR techniques at high magnetic fields, providing valuable structural information at the atomic-level about the fibril architecture. The secondary structures of both fibril types, determined by the assignment of ∼80% of the backbone resonances of these 100- and 94-residue proteins, respectively, reveal substantial backbone rearrangement compared with the location of β-strands in their native immunoglobulin folds. The identification of seven β-strands in hβ_2m fibrils indicates that approximately 70 residues are in a β-strand conformation in the fibril core. By contrast, nine β-strands comprise the fibrils formed from ΔN6, indicating a more extensive core. The precise location and length of β-strands in the two fibril forms also differ. The results indicate fibrils of ΔN6 and hβ_2m have an extensive core architecture involving the majority of residues in the polypeptide sequence. The common elements of the backbone structure of the two proteins likely facilitates their ability to copolymerize during amyloid fibril assembly.

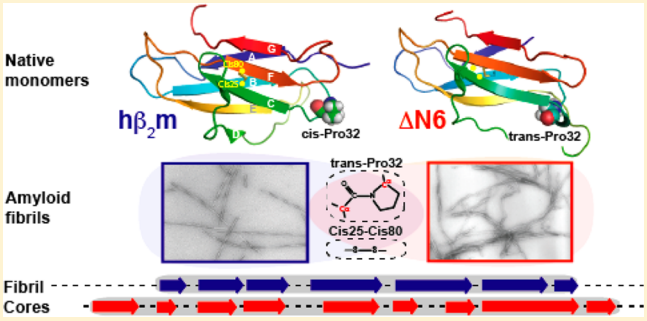

INTRODUCTION

Pathological amyloid fibrils are formed by the misfolding and self-assembly of proteins and peptides such as A$\beta_{40/42}$ in Alzheimer's disease (AD), α-synuclein in Parkinson's disease (PD), islet amyloid polypeptide (IAPP or amylin) in type II diabetes mellitus, and human β_2-microglobulin (hβ_2m) in dialysis-related amyloidosis (DRA).[1−3] Despite the distinct amino acid compositions of amyloid proteins, the self-assembled fibrils adopt a universal and underpinning cross-β molecular structure composed of arrays of ribbonlike β-sheets running parallel to the long axis of the fibrils.[4−6] The structural basis of these filamentous aggregates needs to be investigated to provide a mechanistic understanding of their role in pathological events and to develop therapeutic strategies against protein aggregation diseases. One avenue toward this end is the determination of the molecular structure of the final fibril aggregates. Magic angle spinning (MAS) NMR spectroscopy has demonstrated its indispensable role in elucidating the backbone conformations, supermolecular organization and registry of interstrand arrangements of amyloid fibrils, which otherwise are inaccessible by most common techniques. Indeed, models have been established for a number of amyloid fibrils primarily based on MAS NMR analysis of fibrils formed *in vitro*, including Aβ(1−40),[7−9] α-synuclein,[10−12] Sup35p,[13,14] human prion protein,[15,16] and other protein sequences.[6,17] In addition, MAS NMR and cryo-electron microscopy (cryoEM) were used to determine the complete high-resolution structure of three polymorphs of amyloid fibrils formed by a peptide from transthyretin (TTR$_{105-115}$).[18−20]

Two amyloid fibril components, 99-residue hβ_2m and its truncated variant ΔN6 that lacks the N-terminal six amino acids,[21] are found in osteoarticular amyloid deposits in dialysis-related amyloidosis (DRA). Full-length hβ_2m is remarkably intransigent to fibril assembly at physiological pH and temperature in the absence of cosolvents or other additives.[22] A number of factors, including pH, metal ions, and biologically relevant molecules including collagen, glycosaminoglycans, lysophosphatidic acid, and nonesterified fatty acids induce the fibril formation of hβ_2m *in vitro*.[23−29] For example, at pH 2.5,

Received: December 11, 2013
Published: March 28, 2014

 © 2014 American Chemical Society dx.doi.org/10.1021/ja4126092 | J. Am. Chem. Soc. 2014, 136, 6313−6325

predominantly unfolded hβ_2m protein associates rapidly *in vitro* to form amyloid fibrils.[30] In contrast with the requirement for denaturing or destabilizing conditions to induce fibril formation of the wild-type protein, ΔN6 readily forms fibrils *in vitro* from an initially "folded" monomeric state at pH 6.2−7.2.[31,32] Most recently, even trace amounts of ΔN6 (1%) have been found to facilitate the fibril formation of the natively structured wild-type protein *in vitro* at pH 6.2−7.2.[31] The possession of *trans*-P32 in native ΔN6 rationalizes, in part, the ability of this protein to form amyloid on the basis of its structural similarity to the transient folding intermediate (I_T) identified as a key precursor in amyloid assembly of hβ_2m.[31,33,34] These findings, together with the natural occurrence of ΔN6 in fibrils *in vivo*, have resulted in increasing attention on this variant,[31,32] despite the absence of a consensus as to whether the truncated protein originates prior to, or post, fibril assembly *in vivo*.[35,36] Therefore, hβ_2m and ΔN6 provide an interesting pair of proteins by which to study the mechanisms of amyloid assembly at a fundamental level.[31,32,37]

Since the identification of hβ_2m as an amyloid protein more than 20 years ago, numerous biochemical and biophysical studies have investigated the structure and dynamics of the protein under different solution conditions. X-ray crystallography and solution NMR have provided high-resolution structures of the native, monomeric wild-type protein, which shows a β-sandwich fold consisting of seven antiparallel β-strands, stabilized by a single interstrand disulfide bond.[31,38−42] Other studies focusing on the characterization of precursors (i.e., the native monomer and its partially folded intermediates), fragments, mutated variants, and oligomers of the wild-type protein, have improved our understanding of the nature of the self-assembly mechanisms of hβ_2m into amyloid fibrils.[43−45] However, due to the complexity of the cross-β superstructure and the insoluble and noncrystalline nature of these amyloid assemblies, atomic-level information on structures within the fibril architecture remains elusive. A limited number of pioneering studies have been conducted; for example, Iwata et al. have successfully determined the tertiary structure of a 22-residue segment of hβ_2m (S20−K41) within amyloid fibrils primarily by using MAS NMR,[46] while Eisenberg and co-workers have focused on different 7-residue peptides, from the hβ_2m sequence, that form 3D crystals.[47] However, fibrils formed from a short peptide fragment are insufficient to represent the structural features of the intact protein since the remaining residues not included in the S20−K41 fragment have been found to be crucial in the assembly of the intact protein into fibrils using EPR, mutagenesis, cryoEM, and solution NMR.[31,48−51] The identification of the fibril cores, and therefore residues that are crucial in the fibril assembly, was investigated by H/D exchange[48,52,53] and limited proteolysis experiments.[54,55] Both techniques provide a global profile of protein segments, showing solvent protection or exposure, and the distribution of preferential proteolytic sites. However, neither of these approaches addresses the residue-specific conformational composition of the fibril core. Thus, information elucidating the backbone rearrangement occurring on the pathway of amyloid assembly from the native structure to fibrils, is still missing. Therefore, an atomic-level structure of full-length hβ_2m and ΔN6 in their fibril forms is necessary in order to understand the hierarchical assembly of these elementary building blocks into the complex fibril architecture imaged by cryoEM.[56]

We have recently reported the MAS NMR characterization of full-length hβ_2m fibrils formed at pH 2.5,[57] resulting in the prediction of torsion angles for 40 residues of this 100-residue protein (the recombinant protein contains an additional N-terminal methionine, denoted here as M0). These results suggested at least five segments of β-strands in the fibril structure. The resonance assignments also revealed that H31−P32 peptide bond adopts a *trans*-conformation in hβ_2m fibrils, consistent with *cis*-to-*trans* isomerization of this residue being an important initiating event in fibril formation.[34] However, a clear picture of the secondary structural content of hβ_2m fibrils requires complete assignment of the backbone resonances of the protein in fibrillar form. In addition, no detailed structural studies of the fibrils formed from ΔN6 have yet been performed. Here we present the assignment of backbone resonances of hβ_2m and ΔN6 fibrils (80% and 88% complete, respectively) using a combination of variously isotopically labeled samples and a set of multidimensional NMR techniques at 750−900 MHz. The resulting atomic-level comparison of the secondary structure within the fibrils formed from these proteins reveals structural differences that explain their ability to copolymerize at neutral pH.[32]

MATERIALS AND METHODS

Protein Preparation and Fibril Formation. Biosynthesis and purification of hβ2m and ΔN6 followed protocols as described previously.[31,57] The proteins were isotopically labeled using different strategies for MAS NMR experiments. Briefly, recombinant proteins were expressed in BL21(DE3) pLysS *E. coli* in the presence of HCDM1 minimal media. Three different isotopically labeled samples were prepared for each protein, including one uniformly $^{15}N,^{13}C$-labeled protein and two site-directed ^{13}C- and uniformly ^{15}N-labeled proteins. These three protein samples were produced in minimal media enriched with 1 g/L $^{15}NH_4Cl$ and using either 2 g/L D-glucose-$^{13}C_6$ (named as U-hβ_2m or U-ΔN6), [1,3-^{13}C]-glycerol (1,3-hβ_2m or 1,3-ΔN6) or [2-^{13}C]-glycerol (2-hβ_2m or 2-ΔN6). All isotopes were purchased from Cambridge Isotope Laboratories (Andover, MA) and used without further purification.

The hβ_2m and ΔN6 fibrils were prepared by incubation in a 96-well plate (Corning Incorporated, Costar) in a BMG Fluostar Optima plate reader at 37 °C with constant shaking at 600 rpm. Fibril growth was performed using 0.5 mg/mL soluble protein, 0.02% (w/v) NaN_3 and different pHs and salt concentrations, i.e. 10 mM sodium phosphate buffer containing 50 mM NaCl at pH 2.5 for hβ_2m and 50 mM MES buffer containing 120 mM NaCl at pH 6.2 for ΔN6. The hβ_2m and ΔN6 fibrils were harvested after incubation for approximately 14 or 7 days, respectively. The fibrils were centrifuged at 14,000*g* for 20 min and characterized by negative stain transmission electron microscopy (EM). The fibrils were prepared without seeding, and the consistency of the fibril type was confirmed by analysis of NMR chemical shifts.

Solid-State NMR Experiments. The hydrated fibrils were ultracentrifuged for 24 h at 300000*g* to pack the pellet into 3.2 mm Bruker zirconia rotors (Bruker BioSpin, Billerica, MA). The packed hydrated fibril samples have negligible water loss as monitored by the ^{1}H signal of H_2O. MAS NMR experiments were performed on a custom-designed 750 MHz spectrometer (courtesy of Dr. David J. Ruben, Francis Bitter Magnet Laboratory, Cambridge, MA), and Bruker 800 and 900 MHz spectrometers (^{1}H frequency).

Complete experimental details for the multidimensional MAS NMR experiments are included in the Supporting Information (SI). Briefly, three different kinds of 1D ^{13}C experiments were conducted, including dipolar-coupling based cross-polarization (CP), direct polarization (DP), and scalar-coupling (J)-based INEPT. Two-dimensional (2D) homonuclear $^{13}C-^{13}C$ correlations were recorded using radio frequency-driven recoupling (RFDR), either in a broadband or band-selective manner.[59−61] Two-dimensional heteronuclear $^{15}N-^{13}C$ correlations were achieved by Z-filtered transferred-echo

dx.doi.org/10.1021/ja4126092 | J. Am. Chem. Soc. 2014, 136, 6313−6325

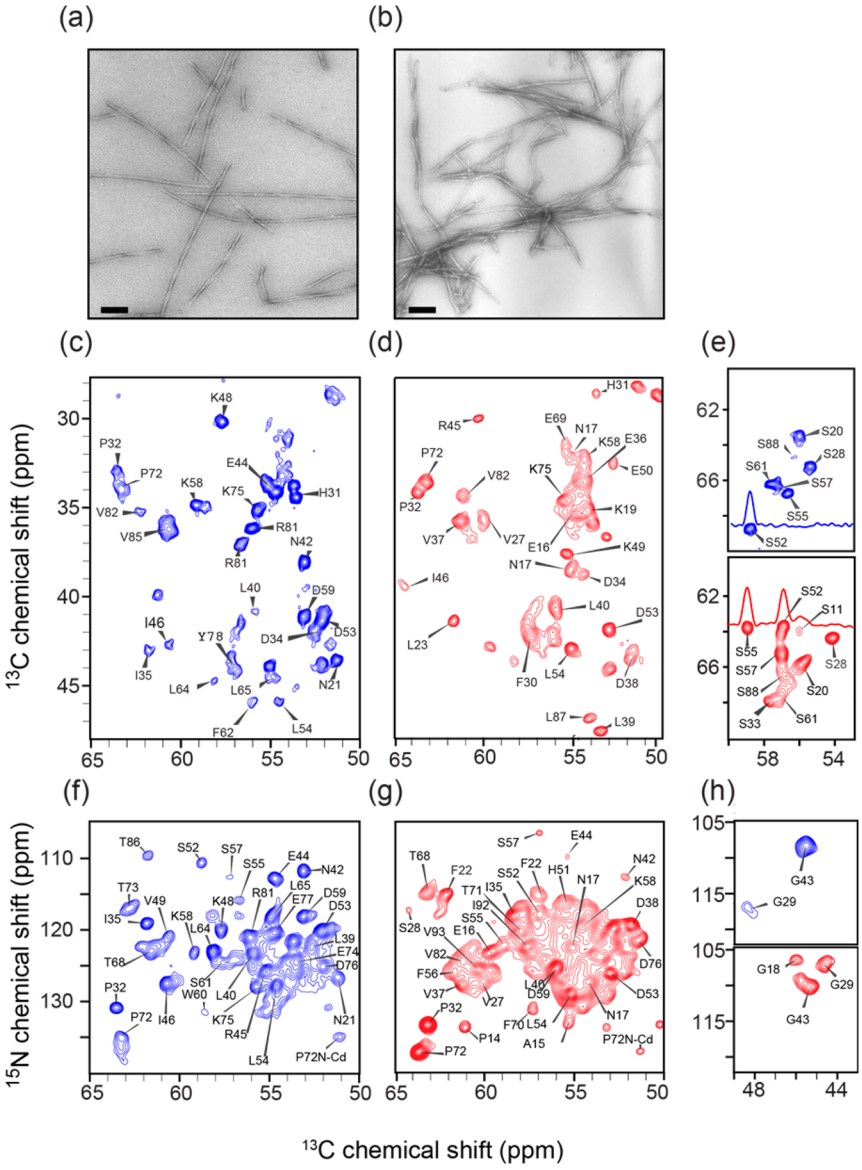

Figure 1. Spectroscopic characterization of hβ_2m and ΔN6 fibrils. Negative stain electron micrographs (EM) of (a) hβ_2m and (b) ΔN6 fibrils (scale bar 100 nm) and their MAS NMR spectra of (c–e) ^{13}C–^{13}C and (f–h) ^{13}C–^{15}N correlations. (c–e) One-bond RFDR spectra of U–^{13}C,^{15}N-hβ_2m (blue) and U–^{13}C,^{15}N-ΔN6 (red). The cross sections of S52 are shown in (e) to illustrate the peak intensity and line width. (f–h) One-bond ZF TEDOR spectra of 1,3-hβ_2m (blue) and 1,3-ΔN6 (red). (c–e) and (f–h) were acquired at 900 and 800 MHz ^{1}H frequencies, respectively. Assignments in spectra are residue-specific and are based on 2D and 3D experiments.

double-resonance (ZF TEDOR)[62,63] and proton-assisted insensitive nuclei cross-polarization (PAIN-CP).[64] Two categories of 3D ^{15}N–^{13}C–^{13}C experiments were performed for sequential assignments, including the conventional N–C–C experiments, i.e. NCOCX, NCACX, and CONCA, and the most recently designed TEDOR-CC experiments.[65,66]

All spectra were processed with NMRPipe.[68] Zero filling and Lorentzian-to-Gaussian apodization for each dimension were applied before Fourier transformation. Polynomial baseline correction in the frequency domain was applied to the detection dimension. A line broadening of 30–60 Hz was used for all 2D and 3D experiments. Peak identification and assignment were performed with Sparky (T. D. Goddard and D. G. Kneller, SPARKY 3, University of California, San Francisco). Protein structures were visualized in PyMOL (The PyMOL Molecular Graphics System, version 1.5.0.4, Schrödinger, LLC.). The assigned N/CO/Cα/Cβ chemical shifts were used as input for the TALOS+ program to predict backbone torsion angles (ϕ, ψ).[69]

RESULTS

High Degree of Conformational Homogeneity of hβ_2m and ΔN6 Fibrils. Obtaining homogeneous samples of amyloid fibrils is an essential priority to ensure high-resolution spectra that enable structural analysis. Figure 1 shows negative stain EM (a,b) and 2D MAS NMR spectra (c–h) of hβ_2m and ΔN6 fibrils, revealing the sample homogeneity as well as spectroscopic differences of the two fibril types. EM images of negatively stained preparations of hβ_2m (pH 2.5, 50 mM NaCl) and ΔN6 (pH 6.2, 120 mM NaCl) show a predominantly homogeneous population of long, straight fibrils with no amorphous aggregates present, consistent with previous results.[32,57] In order to examine the conformational homogeneity of the fibrils further, we recorded 2D MAS NMR spectra using RFDR and ZF-TEDOR sequences selective for one-bond ^{13}C–^{13}C (Figure 1c–e) and ^{13}C–^{15}N (Figure 1f–h) couplings.

dx.doi.org/10.1021/ja4126092 | J. Am. Chem. Soc. 2014, 136, 6313–6325

The spectra exhibit excellent resolution, in which ^{13}C and ^{15}N line widths are ~0.5 ppm and ~0.9 ppm for backbone $^{13}C\alpha$ and ^{15}N resonances, respectively, and ~0.35 ppm for side-chain methyl carbon peaks for both samples.

Despite the similarly high degree of conformational homogeneity of the hβ_2m and ΔN6 fibril samples, a comparison of the spectra reveals differences in the number of cross peaks and their resonance positions. For example, the spectrum shown in Figure 1e of the ΔN6 fibrils displays all 9 serine $^{13}C\alpha$-$^{13}C\beta$ cross peaks, whereas two are absent in the spectra of hβ_2m. Similarly, all three glycine residues (G18, G29, and G43) are present in the backbone $^{15}N-^{13}C$ correlations of ΔN6 fibrils, but only a single, strong cross peak (G43) and a weak one (G29) appear in spectra of hβ_2m fibrils (Figure 1h). The presence of the additional cross peaks in the spectra of ΔN6 fibrils qualitatively suggests a more rigid backbone in the truncated variant. Furthermore, those cross peaks displaying low intensity (e.g., S88 of hβ_2m (Figure 1e (blue)) and S11 of ΔN6 (Figure 1e (red)) or peak broadening (G43 of ΔN6 (Figure 1h (red)) suggest that these residues are in relatively dynamic local regions in the fibril structure, i.e. flexible terminals, turns, or loops. The fact that the fibrils of hβ_2m and ΔN6 differ in the position of their N/Cα/Cβ resonances suggest possible structural differences, which are likely the result of the different lengths of the protein sequences and the different pHs (2.5 and 6.2) employed in the fibril growth. However, to rigorously compare the conformational differences between hβ_2m and ΔN6 fibers, the secondary structure needs to be determined from complete assignments.

In Figure 2, we illustrate ^{13}C cross-polarization (CP) and direct polarization (DP) spectra of hβ_2m and ΔN6 fibrils at 313 K. The efficiency of magnetization transfer in dipolar-based CP experiments largely depends on the rigidity of the sites, while DP spectra sample regions which exhibit short ^{13}C T_1's. The overall CP enchantment factor (ε_{CP}) is around 2.1−2.5 for both fibril samples, which is comparable to the values found for the largely immobile protein DsbB,[70] protein G B1 domain in microcrystals[71] and PI3-SH3 amyloid-like fibrils.[17] In contrast, inefficient CP enhancement (ε_{CP} = ~0.7) was found for the largely mobile α-synuclein fibrils at 273 K.[72] We note that the overlaid 1D ^{13}C spectra of ΔN6 fibrils with (black) and without (red) $^{1}H-^{13}C$ CP transfer, in Figure 2b, show similar spectral features. We observed INEPT signals at 313 K for hβ_2m fibrils, indicative of subnanosecond backbone motions (Figure 2a), as assigned previously[57] to arise from spin systems (identified from the through-bond TOBSY spectra) as the N-terminal seven residues, MIQRTPK. ΔN6 fibrils, truncated at K6, show no INEPT intensity (Figure 2b). These observations exclude the possibility that the two proteins possess large reorientational dynamics in their amyloid forms at the temperature employed (313 K).

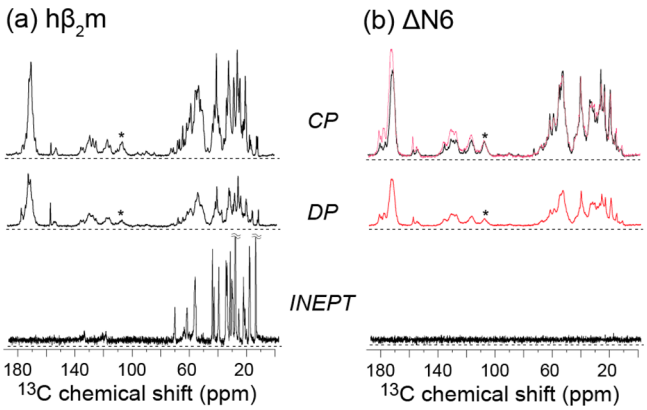

Figure 2. Comparison of 1D ^{13}C spectra of (a) hβ_2m and (b) ΔN6 fibrils at 313 K using cross-polarization (CP, top), direct polarization (DP, middle) and INEPT (bottom). In the case of ΔN6 we superimposed the traces from DP (red) and CP (black) to illustrate that the spectral features are largely preserved. The intensities were scaled to match in the alphatic region. Each CP and DP spectrum was recorded with 16 scans, while each INEPT spectrum required 64 scans. All spectra were collected at 13 kHz MAS frequency, 100 kHz ^{1}H TPPM decoupling, and at 800 MHz ^{1}H frequency. The $^{1}H-^{13}C$ CP contact time was ~1.5 ms, and the recycle delay for the DP and INEPT spectra was 5−5.5 s.

^{13}C and ^{15}N Resonance Assignment of hβ_2m and ΔN6 Fibrils. We next aimed to determine the secondary structures of hβ_2m and ΔN6 fibrils using MAS NMR spectra, and the initial step is the assignment of the individual resonances in the protein sequences. In this study, we employed two established strategies to complete the resonance assignment. First, we performed a set of one-bond and multibond 2D $^{13}C-^{13}C$ and $^{13}C-^{15}N$ correlation experiments to identify the spin systems and to establish partial inter- and intraresidue connections. Samples of hβ_2m and ΔN6 fibrils with uniform ^{13}C, ^{15}N-labeling or labeling with ^{15}N and 2-$^{13}C_1$-glycerol or 1,3-$^{13}C_2$-glycerol (see Materials and Methods) were used. Second, 3D $^{15}N-^{13}C-^{13}C$ spectra were recorded using uniformly ^{13}C,^{15}N-labeled proteins. The sequential assignment process involves the use of one-bond $^{13}C-^{13}C$ and $^{15}N-^{13}C$ correlation experiments to identify residues with characteristic chemical shifts and specific labeling patterns in 2- and 1,3-samples, as discussed below. The inter-residue multibond correlation spectra were used to identify the connectivity of individual residues with the immediately neighboring residues, giving a number of sequential assignments. Those residues assigned in 2D spectra then served as anchor points to facilitate the backbone assignments that map the sequential connectivity. The match of sequence-specific assignments obtained in the comprehensive set of 2D and 3D spectra minimizes the ambiguity in the trial assignments.

Uniform ^{13}C,^{15}N-labeling is the customary initial step in the spectral assignment process since it generally yields spectra with high signal-to-noise ratio. However, the simultaneous labeling of all carbon sites results in significant cross peak overlap, a problem that is exacerbated for relatively large proteins and protein assemblies. This problem stimulated the use of sparse labeling strategies using [1-^{13}C]-glucose, [2-^{13}C]-glucose, [2-$^{13}C_1$]-glycerol or [1,3-$^{13}C_2$]-glycerol as the sole ^{13}C source. The reduced number of labeled sites can greatly simplify spectra; for example, [2-$^{13}C_1$]-glycerol labels the Cα site for residues including G, S, W, F, Y, A, V, and L.[73,74] In contrast, these residues have ^{13}C labeling at ^{13}CO and $^{13}C\beta$ sites for protein samples prepared from *E. coli* grown on [1,3-$^{13}C_2$]-glycerol. As illustrated in SI Figure 1a−c, hβ_2m fibrils labeled with [2-$^{13}C_1$]-glycerol or [1,3-$^{13}C_2$]-glycerol have relatively higher Cα and Cβ intensity, respectively, in agreement with the expected labeling pattern. Concurrently, the ^{13}C line width is reduced due to the abolition of one-bond $^{13}C-^{13}C$ dipolar and scalar couplings in the specifically labeled samples. The removal of the one-bond dipolar couplings also attenuates dipolar truncation from homonuclear dipolar couplings, resulting in better recoupling efficiency between inter-residue spins[75] (see

dx.doi.org/10.1021/ja4126092 | J. Am. Chem. Soc. 2014, 136, 6313−6325

the expanded region at approximately 15 ppm in SI Figure 1b and c).

Figures 3, 4 and 5 illustrate the identification of some of the spin systems, as well as partial sequential connectivity in 2D

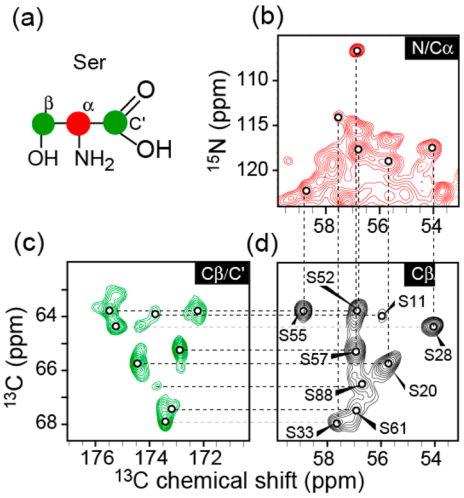

Figure 3. Identification of serine residues of ΔN6 fibrils using 2D MAS NMR and variously labeled samples. (a) ^{13}C-labeling scheme of serine using [2-^{13}C]-glycerol (red) or [1,3-^{13}C]-glycerol (green) as the carbon source.[74,76] (b) One-bond ZF-TEDOR of [2-^{13}C-glycerol]-ΔN6. (c) Multibond RFDR of [1,3-^{13}C-glycerol]-ΔN6 using an 11 ms mixing period. (d) One-bond RFDR of U−^{13}C, ^{15}N-labeled ΔN6 recorded using a 1.6 ms mixing period. Spin systems of all nine serine residues were identified by their characteristic downfield Cα and Cβ chemical shifts. The assignments were from the following 2D and 3D spectra. Dashed lines guide the assignment of each residue.

spectra of hβ_2m and/or ΔN6 fibrils. Using the serine residues as an example (Figure 3a), 1,3-hβ_2m and 1,3-ΔN6 samples contain ^{13}C-labeled CO and Cβ carbons, and only the Cα sites are labeled in samples prepared from growth on 2-glycerol. All nine serine residues of ΔN6 fibrils have been successfully identified from Cβ−Cα cross peaks in a one-bond RFDR spectrum of U-ΔN6 (Figure 3d). Their N−Cα and Cβ−C′ correlations appear in one-bond ZF TEDOR spectra (Figure 3b) and in the multibond RFDR spectrum of the 1,3-sample (Figure 3c), respectively. Other residues including Pro, Gly, and Thr show fingerprint chemical shifts in 2D ^{15}N−^{13}C correlation spectra. More examples can also been found in Figure 4c and d, e.g. all three glycines in ΔN6 fibrils were identified on the basis of the cross peaks of the upfield ^{15}N and ^{13}Cα chemical shifts (Figure 4b).

Two-dimensional MAS NMR has been used successfully to accomplish backbone and side-chain assignment.[77,78] Here we show that the combination of variously labeled samples of hβ_2m and/or ΔN6 fibrils and 2D NMR experiments has enabled the identification of amino acid spin systems and their sequential connectivity for both hβ_2m and ΔN6 fibril samples, despite being 100 and 94-residue proteins, respectively. Figure 4a illustrates four inter-residue correlations that can be established to connect the assignment of atoms in neighboring residues. In the 2-hβ_2m and 2-ΔN6 protein samples, ^{15}N−^{13}C and ^{13}C−^{13}C correlations including one-bond ^{15}N(i)−^{13}C′(i − 1) and multibond ^{15}N(i)−^{13}Cα/β(i − 1), ^{13}Cα(i)−^{13}Cα(i ± 1) and ^{13}C′(i)−^{13}Cα(i − 1) correlations can be established by using ZF TEDOR with short or long mixing times, and RFDR experiments, respectively. Unbroken blue and violet lines in Figure 4b−e guide the partial or complete connectivity of consecutive segments comprising residues S55 to K58 and S28 to D34 of ΔN6 fibrils, respectively. Colored and broken lines correlate the same residues in different spectra. Different lengths of the mixing time were used to correlate one- or multibond spins as described in the experimental details in the Supporting Information. To avoid dipolar truncation from one-bond spin pairs and to allow efficient detection of the coupling of distant spin pairs, the use of both the 2- and 1,3-glycerol labeled samples is required. Sequential assignments from S28 to D34 of ΔN6 fibrils were established from ^{15}N(i)−^{13}Cα(i + 1) and ^{15}N(i)−^{13}Cα/β(i − 1) correlations in Figure 4b and c, respectively. The same connections can be identified from ^{13}Cα−^{13}Cα correlations in Figure 4d. The ^{13}C labeling at Cα sites for the majority of residues in 2-ΔN6 facilitates the detection of such weak dipolar coupling, which otherwise is difficult to detect. We used long-mixing RFDR (τ_{RFDR} = 16.2 ms) to establish the inter-residue ^{13}Cα−^{13}Cα correlations. A low-power (12.5 kHz) rectangular π pulse was used in the dipolar recoupling to selectively excite the aliphatic carbons, which has been shown to provide better efficiency.[61,79] Besides the sequential ^{13}Cα−^{13}Cα correlations, the connectivity of adjacent residues in the spectra of ΔN6 fibrils was also established from ^{13}C′(i)−^{13}Cα(i − 1) contacts (Figure 4e).

In order to overcome the difficulty of peak overlap in 2D spectra required to obtain near-complete assignments of hβ_2m and ΔN6 fibrils, the extension to one more spectral dimension is necessary. Two categories of 3D experiments, distinguished by the N−C magnetization transfer, were performed to obtain unambiguous sequential assignment. The first category of experiments, including NCOCX, NCACX and CONCA, utilizes band-selective SPECIFIC-CP to transfer magnetization between ^{15}N and ^{13}CO, or between ^{15}N and ^{13}Cα.[80−84] Taking the 3D NCOCX experiment for example (as illustrated by the green route in Figure 5a), the magnetization was initiated from the amide ^{1}H of residue i and transferred to the directly bonded ^{15}N via CP. Subsequently, a SPECIFIC CP mixing sequence is utilized to transfer the magnetization from N to C′ of its preceding residue i − 1. Finally, the homonuclear ^{13}C−^{13}C correlations are established via spin diffusion. NCACX correlates the intraresidue backbone to side-chain carbons of residue i, while CONCA realizes the connectivity of residue i to its succeeding neighbor i + 1. Reasonably good transfer efficiencies of 35−45% were obtained, which again suggests the high rigidity of the majority of the protein backbone of both hβ_2m and ΔN6 fibrils.[70,82] Figure 5b shows representative strip plots of the ^{13}C−^{13}C planes of the three 3D NCC spectra of ΔN6 fibrils, providing an indication of the spectral quality. The plot consists of strips from three 3D spectra: NCOCX (green), NCACX (blue), and CONCA (red). The sequential connectivity from S52 to K58 is established by N/CO/Cα/Cβ as well as side-chain carbons. Residues including Ser and Thr are easily identified by the downfield Cα/β chemical shifts. The side-chain ^{13}C chemical shifts can also serve as an identifier of residues including Lys, Arg, Glu, Gln, and Ala. Examples of the side-chain assignment walks in NCOCX (green) and NCACX (blue) spectra include well-resolved peaks of D53 Cγ (178.1 ppm), L54 C$\gamma/\delta1/\delta2$ (30.2 ppm, 27.6 ppm, 25.0 ppm, respectively), and K58 C$\gamma/\delta/\varepsilon$ (25.4 ppm, 29.9 ppm, 42.3 ppm, respectively). Sequential connectivity for the same region is observed in 2D spectra as guided by blue lines in Figure 4, providing additional verification. The same connectivity for

dx.doi.org/10.1021/ja4126092 | J. Am. Chem. Soc. 2014, 136, 6313−6325

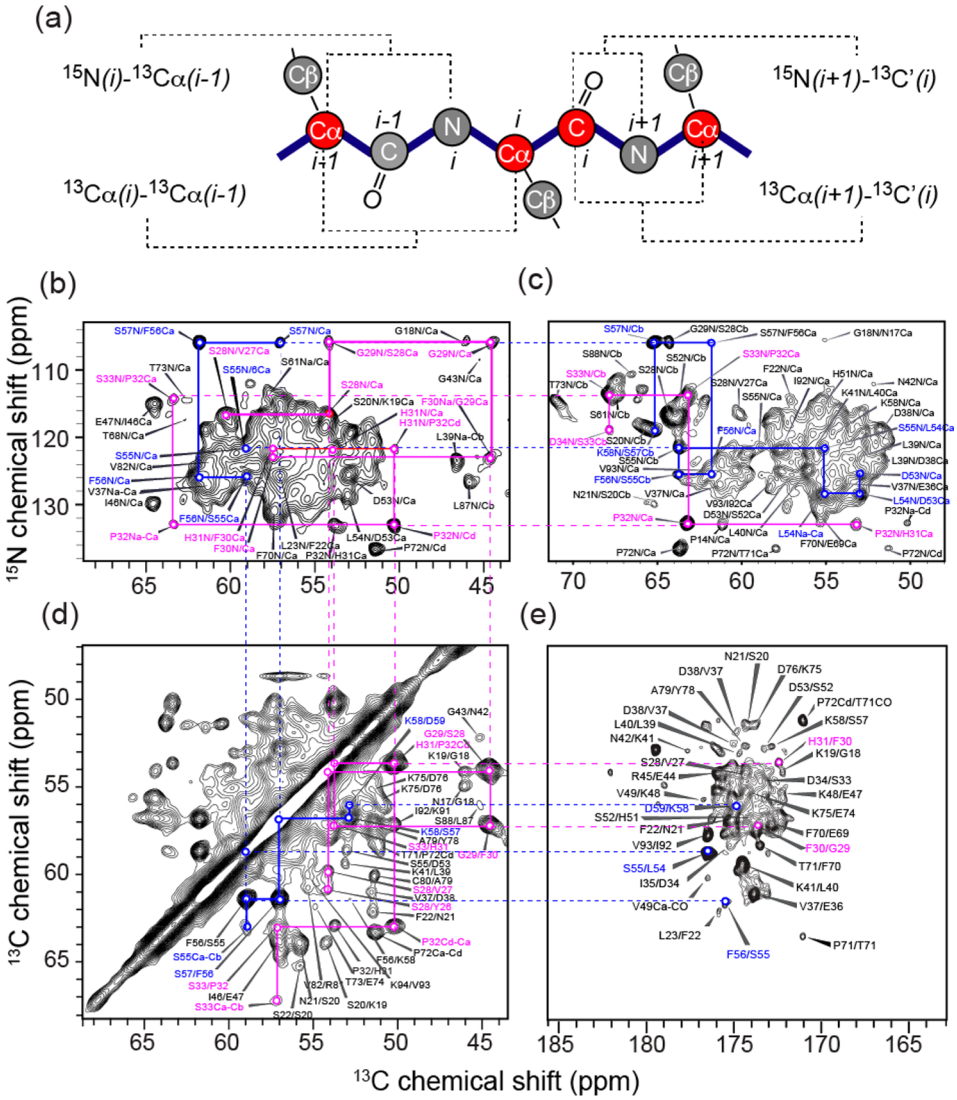

Figure 4. Sequential connectivity of ΔN6 fibrils established in 2D correlations. (a) Schematic illustration of the backbone walk that can be obtained through a set of inter-residue $^{13}C-^{15}N$ and $^{13}C-^{13}C$ correlations by using 2-hβ_2m and 2-ΔN6, which has mostly alternating ^{13}C enrichment. (b) Multibond ZF TEDOR spectra of 2-ΔN6, showing representative $^{15}N(i)-^{13}C\alpha/\beta(i-1)$ connections of S55-F56-S57 (blue lines) and S28-G29-F30-H31-P32 (violet lines). (c) Multibond ZF TEDOR spectra of 1,3-ΔN6, showing the $^{15}N(i)$-$^{13}C\alpha/\beta(i\text{-}1)$ connectivity of D53-L54-S55-F56-S57-K58 (blue lines) and H31-P32-S33-D34 (violet lines). (d) Broad-band RFDR showing the $^{13}C\alpha(i)$-$^{13}C\alpha(i \pm 1)$ connectivity of S55−F56−S57-K58 (blue lines) and S28-G29-F30-H31-P32-S33 (violet lines). (e) Band selective-RFDR of 2-ΔN6, showing the $^{13}C'(i)$-$^{13}C\alpha(i-1)$ correlations. (b,c) and (d,e) were acquired on 800 and 900 MHz spectrometers (^1H frequency), respectively.

hβ_2m fibrils is obtained, as illustrated in SI Figure 2, showing similarly good resolution and intensity.

Determination of a *trans*-Conformation of P32 and the Single Disulfide Bridge Linking C25 and C80 in hβ_2m and ΔN6 Fibrils. The *cis*-to-*trans* isomerization of the H31−P32 peptide bond in hβ_2m is intimately involved in the backbone rearrangement required to initiate fibril formation, suggesting that isomerization of the main-chain at residue 32 is mechanistically crucial in fibril assembly.[34,50,85] The ^{13}C chemical shift of proline has been utilized as a reliable sensor to identify the bond conformation of X-Pro.[86,87] For example, the chemical shift difference between Cβ and Cγ ($\Delta C\beta/\gamma$) is normally less than 5 ppm for *trans*-X-Pro but larger than 10 ppm for *cis*-conformers.[86,87] A common difficulty of assigning proline in conventional 3D N−C−C spectra is the weak intensity due to its lack of an N−H group.[88,89] It therefore precludes the assignment of the preceding residue as well, usually causing the incomplete mapping of the secondary structure. We have recently developed a new 3D experiment, TEDOR-CC, specifically to resolve this problem.[65,66] As shown in Figure 6a, the initial magnetization was from the cross-polarization of H−Cα or H−CO, instead of H−N in the 3D spectra illustrated in Figure 5a, ensuring the signal of proline residues. In addition, simultaneous N−CO and N−Cα transfers in TEDOR-CC were achieved using dipolar recoupling π-pulse trains, without requiring high stability for the long and simultaneous irradiation of all ^1H, ^{15}N, and ^{13}C channels in the SPECIFIC-CP mixing. The representative strip plot of 3D TEDOR-CC spectra of U-ΔN6 fibrils is shown in Figure 6b. Reliable connectivity from G29 to S33 was established via the well-matched CO, Cα, and Cβ chemical shifts in distinct NCOCX and NCACX spectra. Two-dimensional planes showing full correlations of all carbons of P32 are included in SI Figure 3.

dx.doi.org/10.1021/ja4126092 | J. Am. Chem. Soc. 2014, 136, 6313−6325

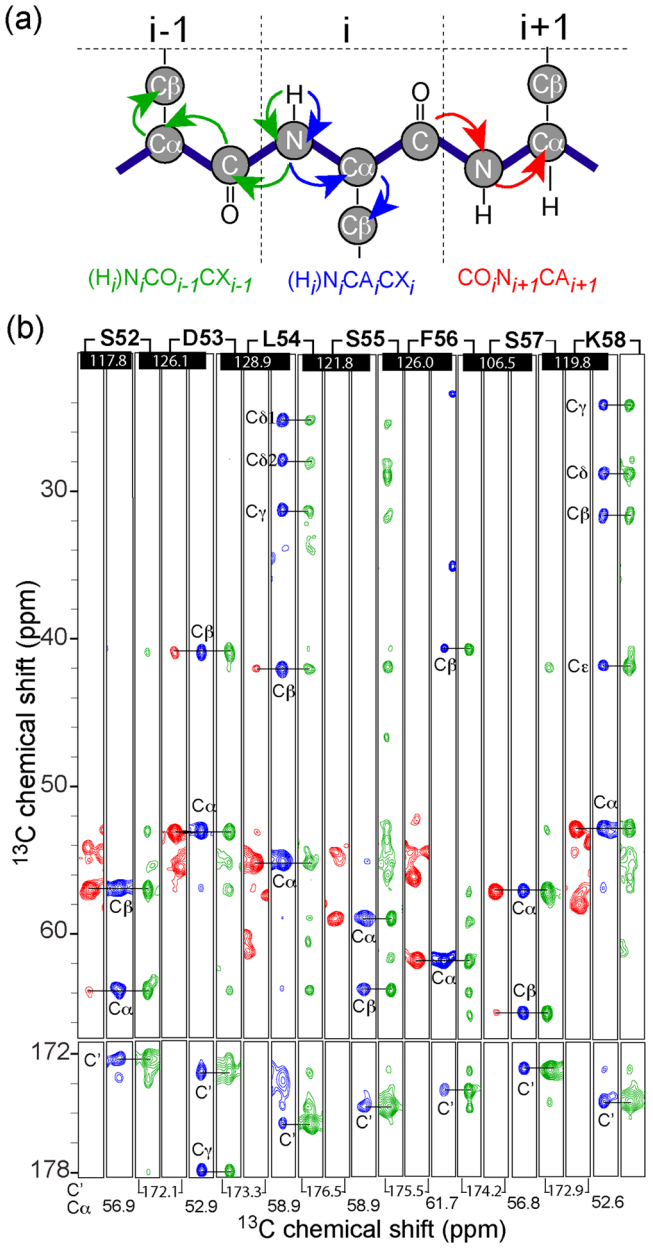

Figure 5. Representative sequential assignments of ΔN6 fibrils from 3D ^{15}N−^{13}C-^{13}C correlation experiments. (a) The inter- or intra-residue magnetization transfer pathways in CONCA (red), NCACX (blue) and NCOCX (green). (b) Backbone walks from S52 to K58 in 3D correlation experiments. ^{15}N chemical shifts where each 2D plane is truncated are listed in black squares. The horizontal axis indicates the CO/Cα chemical shifts. The spectra were acquired using U−[^{13}C,^{15}N-labeled]-ΔN6 fibrils on a 750 MHz spectrometer (^{1}H frequency). A representative strip plot for the same segment of hβ_2m fibrils is shown in SI Figure 2.

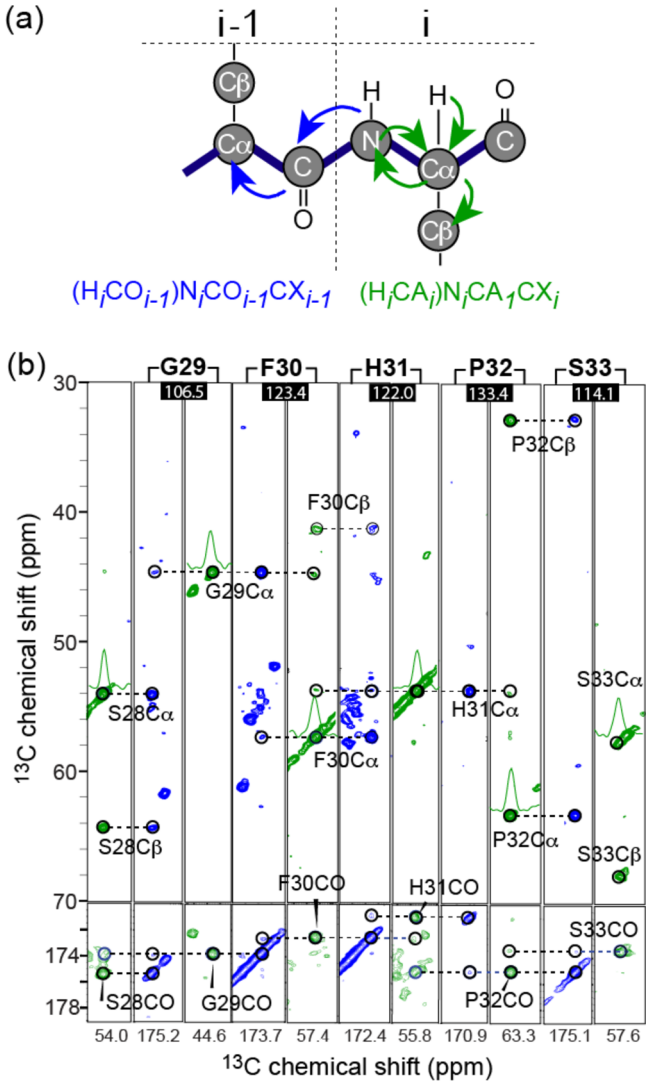

Figure 6. Representative sequential backbone walks from S28 to S33 in 3D TEDOR-CC spectra of ΔN6 fibrils. (a) Simultaneous transfers of N(i)−C′(i − 1) and N(i)−Cα(i). The initial magnetization in TEDOR-CC is from ^{13}C−^{1}H CP, in contrast to the ^{15}N−^{1}H CP in conventional 3D ^{15}N−^{13}C−^{13}C experiments, providing the optimal enhancement of proline intensity. (b) 2D ^{13}C−^{13}C (F1−F3) planes of the 3D TEDOR-CC spectrum of ΔN6 fibrils. ^{15}N chemical shift (F2) for each 2D plane is indicated in black squares. CO and Cα chemical shifts are shown on the x-axis. One-dimensional cross sections are shown for Cα peaks in NCACX spectra in green. Homonuclear ^{13}C−^{13}C mixing was accomplished using 4.8 ms RFDR. The spectra were acquired using the U-ΔN6 fibril on a 900 MHz spectrometer (^{1}H frequency).

Additional verification of the assignment of P32 was from 2D ^{15}N−^{13}C correlation spectra of 2- and 1,3-samples, using the specific patterns of ^{13}C-enrichment, as shown in Figure 7. ^{15}N−^{13}Cα and ^{15}N−^{13}Cδ cross peaks of P32 and P72 are present in the one-bond TEDOR spectrum of U-ΔN6 (Figure 7b), in contrast to the absence of Cδ peaks in 1,3-ΔN6 (Figure 7c), which agrees well with the labeling pattern of proline shown in Figure 7a. The presence of Cγ peaks in the multibond TEDOR spectrum of 1,3-ΔN6 (Figure 7d), while absent in the spectrum of the 2-sample (Figure 7f) verifies the identification of the spin system of proline. The set of 2D spectra in Figure 7 helps to sequentially assign the two proline residues as well. Histidine has ^{13}C enrichment at C′ for the 1,3-ΔN6 and Cα for 2-ΔN6, resulting in P32N−H31C′ cross peaks in the one-bond TEDOR spectrum and P32N−H31Cα in multibond spectra in Figure 7c and Figure 7f, respectively. The unambiguously assigned chemical shifts of P32 in ΔN6 fibrils, together with our previously reported values of the chemical shifts of this residue in the native monomer of ΔN6,[31] and both native and fibril conformations of hβ_2m,[31,57] are shown in SI Table 1. Specifically, $\Delta C\beta/\gamma$ of P32 is 4.3−4.9 ppm for native and

dx.doi.org/10.1021/ja4126092 | J. Am. Chem. Soc. 2014, 136, 6313−6325

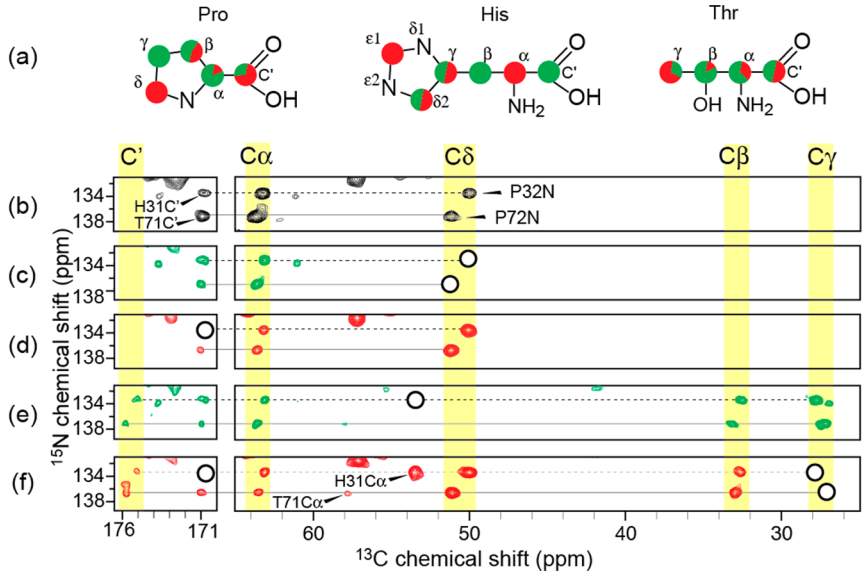

Figure 7. Residue-specific assignment of P32 and P72 of ΔN6 fibrils from 2D ZF TEDOR spectra of proteins labeled at all ^{15}N sites and varied ^{13}C sites by using U−[^{13}C]-glucose, [1,3-$^{13}C_1$]-glycerol or [2-$^{13}C_2$]-glycerol as carbon sources. (a) ^{13}C-labeling scheme of Pro, His, and Thr residues by using [2-$^{13}C_2$]-glycerol (red) or [1,3-$^{13}C_2$]-glycerol (green) as the carbon source. One-bond ZF TEDOR of (b) U-ΔN6, (c) 1,3-ΔN6, (d) 2-ΔN6. Multibond ZF TEDOR of (e) 1,3-ΔN6 and (f) 2-ΔN6. All spectra were acquired at an 800 MHz ^{1}H frequency.

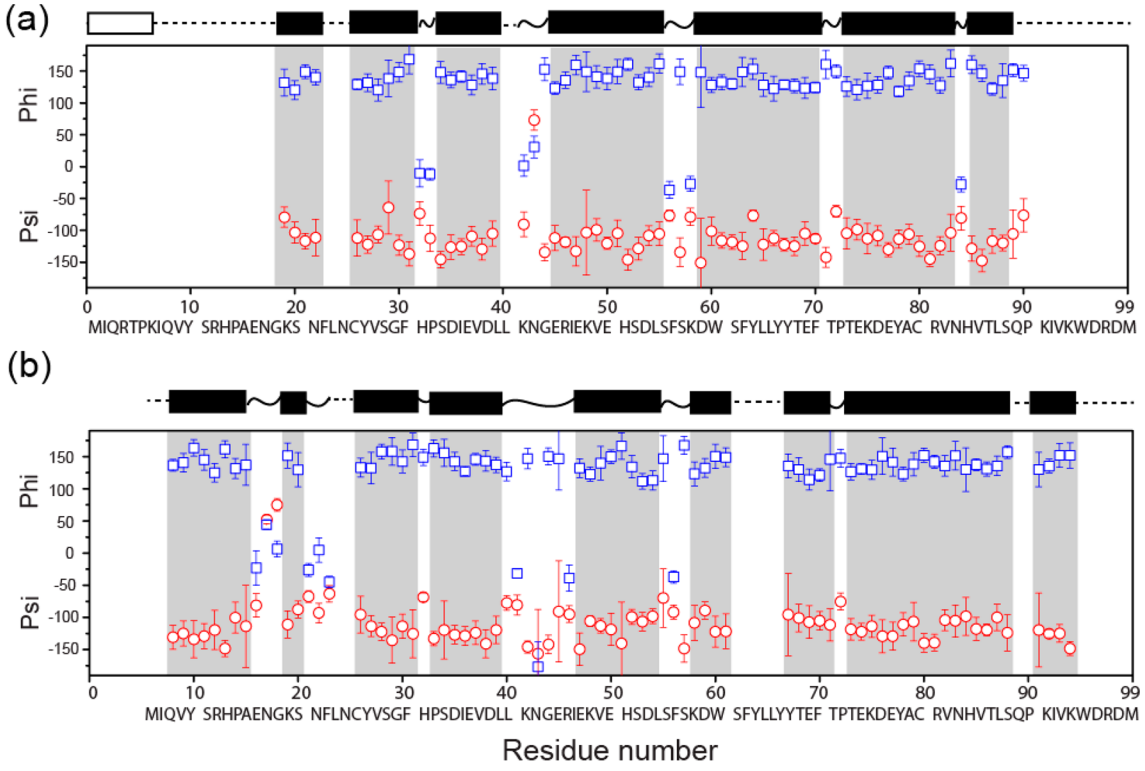

Figure 8. Secondary structure predictions of (a) hβ_2m and (b) ΔN6 in their fibril forms based on TALOS+ analysis of assigned chemical shifts. TALOS+ predicted backbone dihedral angles (phi, blue squares, psi, red circles), with error bars based on the 10 best database matches. The predicted secondary structures are shown at the top of (a) and (b) (β-strands, filled boxes; turn or loop, curved lines; not assigned, dashed line). The white box in (a) depicts the seven residues present in the spectrum of INEPT-based J-TOBSY.[94]

fibrillar ΔN6 and fibrillar hβ_2m, while for native hβ_2m which contains *cis*-Pro32 Δ$C\beta/\gamma$ it is 10 ppm.[31] More rigorously, we compared the C′, Cβ, and Cγ chemical shifts of P32 in ΔN6 fibrils to folded proteins with known X-Pro conformations, confirming assignment of the isomeric status of P32 in the different samples (SI Figure 4).

The disulfide bridge linking C25 and C80 functions as an essential constraint to maintain the hydrophobic core of native hβ_2m and ΔN6.[31,90] To investigate whether this S−S bond is retained in the fibrils formed from hβ_2m and ΔN6, we assigned the chemical shifts of their cysteines. SI Figure 5 shows spectra of 2D ^{15}N−^{13}C PAIN-CP and 3D ^{15}N−^{13}C−^{13}C experiments for the assignment of C80. As a third spin-assisted recoupling

dx.doi.org/10.1021/ja4126092 | J. Am. Chem. Soc. 2014, 136, 6313−6325

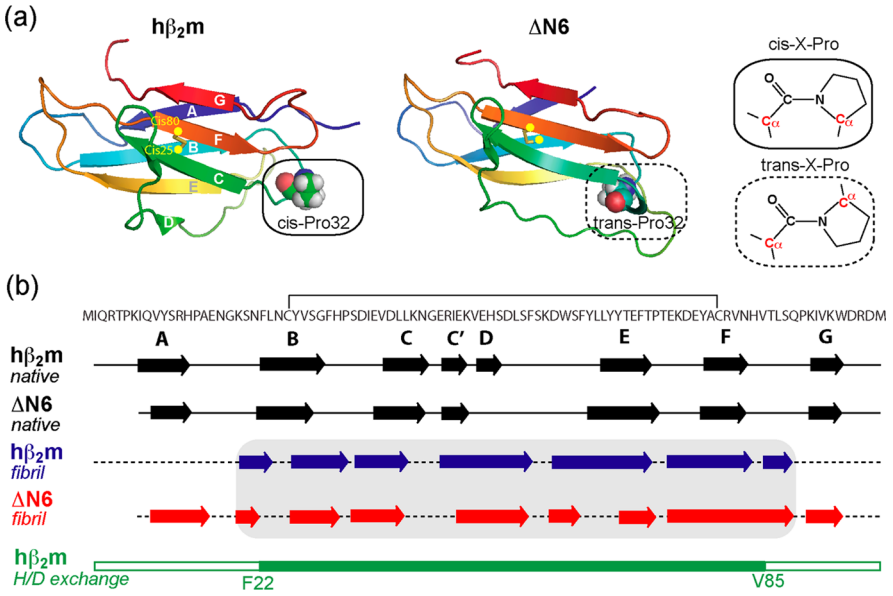

Figure 9. (a) Similar β-sandwich structures of hβ_2m (PDB: 2XKS[31]) and ΔN6 (PDB: 2XKU[31]) monomer in their native forms. The different *cis*- vs *trans*-conformations of P32 are highlighted in squares. (b) Comparison of the secondary structures of hβ_2m and ΔN6 in their native and fibril forms. Arrows indicate β-strands. The secondary structures of hβ_2m and ΔN6 monomers were taken from a solution NMR study by Eichner et al.[31] The H/D exchange plot at the bottom is generated from data of hβ_2m fibrils formed at pH 2.5 by Skora et al.[53] and Hoshino et al.,[48] where filled and open green rectangles indicate residues with greater or less than 60% remaining intensity after exchange at pD 2.5 for 7−8 days at 4 °C and 25 °C, respectively.

(TSAR) technique, PAIN-CP utilizes second-order recoupling and yields efficient long-range ^{15}N−^{13}C correlations.[64] Taking S52 for example, it established correlations with the nearby residue $i \pm 1$ (E50 and H51) and $i \pm 2$ (D53 and L54). Unambiguous assignment of C80 is obtained from the connectivity of A79-C80-R81-V82 in both 2D and 3D spectra (SI Figure 5). The assigned chemical shifts of C80 are summarized in SI Table 1. The chemical shift of Cβ is a good indicator of whether the cysteine is oxidized or reduced.[91] Specifically, a chemical shift value of 34−48 ppm indicates the existence of a S−S bond, while a more upfield value (22−34 ppm) suggests a reduced cysteine.[91] As shown in SI Table 1 and SI Figure 6, the Cβ values of C80 are ∼43 ppm and in the middle of the distribution of Cβ chemical shifts of oxidized cysteine for both hβ_2m and ΔN6 fibrils, suggesting the existence of the disulfide bond. The absence of C25 resonances is likely due to the chemical shift degeneracy in the fibrils of both hβ_2m and ΔN6, ruling out direct analysis of its Cβ shifts.

Secondary Structure Prediction from N/CO/Cα/Cβ Chemical Shifts. The combination of multidimensional MAS NMR techniques and site-specifically labeled samples has greatly facilitated the sequential assignment of backbone atoms of the fibrils formed from hβ_2m at acidic pH (commencing from an acid unfolded state) and from folded ΔN6 at pH 6.2. For hβ_2m, approximately 80% of the backbone resonances were assigned, including 73 residues from CP-based experiments (i.e., 2D ^{13}C/^{15}N−^{13}C and 3D ^{15}N−^{13}C−^{13}C correlation experiments) and 6 from INEPT-based ^{13}C−^{13}C TOBSY.[57] The remaining 21 residues, corresponding to amino acids in the two terminal regions, are unassigned since these resonances are missing in the MAS NMR spectra. For the truncated variant ΔN6, 82 residues out of 94 residues, or 88%, were all assigned from CP-based MAS NMR spectra. The missing resonances of these fibrils are likely due to the intermediate backbone motion on the microsecond to millisecond time scale that has been observed for regions of membrane and amyloid proteins.[72,92,93] Alternatively, dynamic disorder of protein segments could also result in loss of signal intensity due to homogeneous broadening. The assigned resonances served as input into TALOS+ to predict the backbone torsion angles (φ, ψ), as plotted in Figure 8. Secondary structures of hβ_2m and ΔN6 fibrils were determined by the predicted torsion angles and shown on the top of the plot. The hβ_2m fibrils contain seven β-strands, located in the central region (residues K19 to S88) of the protein sequence. Interestingly, these strands appear at similar positions for the ΔN6 fibrils, in spite of slight differences in the boundaries of each segment. Additionally, the ΔN6 fibril structure contains two additional β-strands in the N- and C-terminal regions, a significant difference from the fibril form of the wild-type protein which contains a dynamic N-terminal region. The absence of assignment of residues in the C-terminal region of the hβ_2m fibrils, however, precludes comparison of the structure in this region in the two fibrils types.

DISCUSSION

Site-specific ^{13}C enrichment protocols have been applied extensively to elucidate the structures of insoluble proteins using MAS NMR, including microcrystalline proteins, protein assemblies, membrane proteins, and protein models of amyloid fibrils.[17,65,74,76,95−98] By using a combination of U- and 2- and 1,3-glycerol labeled samples, we have assigned >80% of the residues of fibrils formed from hβ_2m at pH 2.5 and ΔN6 at pH 6.2 and conducted secondary structural analysis of the two fibril forms.

Backbone Rearrangement from Monomeric Proteins to Fibrils: What Is Changed and Unchanged? Fibril formation of native, monomeric hβ_2m is highly dependent on the solution conditions.[99] The fact that this protein forms fibrils under acidic conditions but stays natively folded at neutral pH implies that unfolding of the native protein is a required step in

dx.doi.org/10.1021/ja4126092 | J. Am. Chem. Soc. 2014, 136, 6313−6325

its assembly into amyloid fibrils. Indeed, a significant backbone rearrangement in the assembly of hβ_2m into fibrils has been suggested in many studies using solution NMR, EPR, H/D exchange, and limited proteolysis.[48,51−55] The MAS NMR analysis presented here enables a direct comparison of the secondary structure content of the monomeric and fibrillar forms of hβ_2m and ΔN6 spanning >80% of the protein sequence, and provides the first analysis of fibrils formed from ΔN6, showing distinct changes in the backbone structure between the monomeric and fibril forms for both proteins (Figure 9). Taking natively folded hβ_2m, for example, its β-sandwich structure is composed of two antiparallel β-sheets, one represented by the A-, B-, E-, and D-strands, and the other by the C-, F-, and G-stands (Figure 9a).[31] One of the largest differences between the monomeric and fibrillar structures occurs within the loop regions of hβ_2m in the native form, including B−C, D−E, and F−G loops (Figure 9b), which become part of the β-strands in fibrillar hβ_2m. Specifically, the D−E loop in the native hβ_2m protein forms noncovalent contacts with the MHC I heavy chain[100,101] and is dynamic in the native monomeric protein.[31] Our results indicate that the native D- and E-strands are extended in the fibril form by incorporating residues initially in loops or dynamic regions into β-strands, which lie in the fibril core.[54,55] This validates the hypothesis in many structural studies of monomeric hβ_2m which suggest the potential of these regions to assemble into amyloid fibrils.[40,47,102−107] Conformational rearrangement of residues in the B−C and F−G loops has also been observed in partially folded hβ_2m,[31,34] and these residues are also involved in the formation of β-strands in the fibrils studied here. All these differences for hβ_2m, together with similar observations for ΔN6, suggest significant structural changes occur in the monomer-to-fibril transition for both proteins. Moreover, our results indicate that D-, E-, and F-strands of hβ_2m are extended in length in the fibril form. Despite the presence of seven β-strands in both monomeric native hβ_2m and its fibrillar form, the precise location of the strands differs significantly, suggestive of significant structural differences between the secondary structure of the monomeric and fibril forms. Moreover, considering that the hβ_2m fibrils are formed from an acid unfolded state at pH 2.5 that lacks secondary structure, the results indicate that substantial refolding accompanies self-assembly during the fibril formation of this protein at acidic pH.

Although the β-strands have shifted in location or extended in length in the fibril forms of hβ_2m and ΔN6, the chemical shift analysis presented here suggests that the disulfide bridge involving residues C25 and C80 is preserved in both hβ_2m and ΔN6 fibrils. This finding concurs with previous studies that identified the S−S bond as remaining intact in fibrils formed from hβ_2m and ΔN6 *in vitro*[32] and *in vivo*.[108] The requirement for an oxidized S−S bond for formation of hβ_2m fibrils *in vitro*[90,109−111] suggests its significant role as a fundamental interaction in providing tight intramolecular contact that presumably rigidifies the monomer in fibrils. For example, Katou et al.[111] and Smith et al.[90] have shown that the reduced hβ_2m protein, in which the only disulfide bond is abolished, forms curved and flexible fibrils different from the long straight fibrils formed at acidic pH.

Conformational Differences between hβ_2m and ΔN6 Fibrils Can Explain the Relatively Enhanced Amyloidogenic Potential of the Truncation Variant. ΔN6 can form fibrils at neutral pH, without the acid-induced unfolding required for formation of fibrils from the wild-type protein in the absence of cosolvents or other additives.[31] Such distinct amyloidogenicity can be rationalized, in part, by the different behaviors of the two proteins in monomer and fibril forms. For example, the requirement for the *cis*-to-*trans* transition of the H31−P32 bond in hβ_2m fibril assembly and retention of the *trans*-H31−P32 isomer in fully assembled fibrils was previously reported (Figure 9a).[57] In the current study, we identified the *trans* conformation of H31−P32 in ΔN6 fibrils via chemical shift analysis, the same conformer as in its monomeric form.[31] Proline *cis*-to-*trans* isomerization, a process usually accompanied by conformational rearrangement in a variety of proteins, has been proposed to be a "switch" to trigger the assembly of hβ_2m amyloid fibrils based on the observation of a *trans*-P32 folding intermediate on the fibril formation pathway.[34,42,46,48] The identification of the *trans*-form of H31−P32 in both hβ_2m and ΔN6 fibrils supports this view. From a thermodynamic point of view, P32 in native hβ_2m is trapped in a *cis* conformation by favorable hydrogen bonds and hydrophobic contacts in the native protein. Therefore, partial unfolding of the monomeric structure at acidic pH or by adding denaturants, cosolvents, or Cu^{2+} ions becomes necessary for fibril formation of the wild-type protein. The resulting backbone rearrangement, particularly the increased conformational dynamics of the N-terminal residues, enables the *cis*-to-*trans* isomerization of P32.[31] The dynamic structure of the N-terminal 18 residues in hβ_2m fibrils renders them invisible in dipolar-coupling-based MAS NMR spectra, while these residues have been observed in J-based $^{15}N-^{1}H$ HSQC spectra, suggesting high flexibility of this region on the nanosecond time scale.[53] Low-temperature experiments are necessary to slow or quench the rate of the backbone motion in order to complete the assignments of the terminal residues of hβ_2m fibrils. By contrast with the dynamic terminal regions of fibrils formed from hβ_2m, we show here that ΔN6 fibrils possess a short β-strand within each terminal region of the sequence in a similar location to the A- and G-strands in its native structure (Figure 9b). How these strands pack in the fibrils remains to be determined, although retention of a native-like overall topology is highly unlikely, given the incompatibility of the β-sandwich fold with a cross-β architecture.[112]

The Fibril Core Determined by the Distribution of Rigid β-Strands and Dynamic Domains. The predicted backbone structure of hβ_2m in the amyloid fibrils studied here contains seven β-strands in the region from K19 to S88, indicating an approximately 70-residue fibril core. This is in good agreement with the core region suggested by previous H/D exchange[48,53] and limited proteolysis experiments[54,55] (Figure 9b). Our data further show that the rigid core of hβ_2m fibrils is constrained by an experimentally observed S−S disulfide bond. The high β-strand content found in the fibril core (55 of the 70 residues have φ and ψ angles consistent with a β-strand) provides opportunities for extensive intermolecular hydrogen bonds between stacked monomers, forming a rigid and stable β-sheet core typical of amyloid.[48] The results presented here provide direct identification of residues in hβ_2m and ΔN6 amyloid fibrils, as well as the location of β-strands in the core region, which are essentially inaccessible by other techniques of structural analysis. Such a finding is supported by the observation of different degrees of dynamics throughout the protein sequence. For example, residues in the N-terminal 18 amino acids are absent in dipolar-based spectra of fibrils formed from hβ_2m and instead were identified in spectra of J-based solution-NMR experiments.[53,57] The extensive motion of C-

terminal residues has also been found by studies using EPR.[51] Intriguingly, many features of the fibril core of hβ_2m are conserved in fibrils formed from ΔN6, except that the latter fibrils have β-strands in the N- and C- terminal regions (Figure 9b). Recently, we reported the biophysical characterization of copolymerized hβ_2m and ΔN6 fibrils[32] in which the two proteins copolymerize in heterofibrils in a ∼1:1 molar ratio. The similar core-forming residues in the central region of both proteins, defined by the occurrence and position of β-strands, provide a prerequisite for determining the intermolecular hydrogen-bonding patterns between the two protein components of the copolymer, and may provide a structural rationale for why these two proteins copolymerize so efficiently. Further investigation of the intermolecular packing of the homo- and heteropolymeric fibrils and a comprehensive comparison of their fibril morphology will provide mechanistic understanding of the role of the naturally occurring truncation variant in the assembly pathway and the extent to which the fibril architecture differs in the different fibril forms.

CONCLUSION

In summary, we have determined the location of the β-strand domains of amyloid fibrils of hβ_2m and ΔN6 by utilizing a variety of $^{13}C/^{15}N$-labeling strategies and combining these with multidimensional MAS NMR techniques at high magnetic fields. The results reveal that approximately 70 residues comprise the core of hβ_2m fibrils, distributed into seven β-strands and rigidified by the C25−C80 disulfide bond. By contrast, ΔN6 fibrils contain an additional two β-strands that extend the core region to 87 of the 94 residues in this protein sequence. The relatively more rigid termini of the truncated variant, together with the finding of its natively *trans*-P32 in monomeric and fibril forms, contrasts with the *cis*−*trans* isomerization required for fibril formation of native hβ_2m, and provides a rationale for the enhanced ability of ΔN6 to form fibrils. The assignments (>80% of the protein sequence complete for these 100 and 94 residue proteins) provide a valuable foundation for further investigation of the intermolecular packing between monomers in these different fibril forms and to elucidate the extent to which the structural architecture of the fibril forms differs. To assign the remaining residues whose resonances are absent from current spectra, we are performing experiments at liquid-nitrogen temperature to quench the backbone dynamics, in combination with dynamic nuclear polarization (DNP) techniques for sensitivity enhancement.[113−115] Together this information will inform development of 3D models for the fibril architectures of these different β_2m fibril structures. Such information is essential for understanding how and why fibrils develop in dialysis-related amyloidosis and to develop future strategies to prevent amyloid deposition and disease.

ASSOCIATED CONTENT

Supporting Information

Experimental details concerning the following. One-dimensional MAS characterization of fibril samples with different ^{13}C-labeling patterns; representative strip plot of 3D $^{15}N-^{13}C-^{13}C$ spectra of ΔN6 fibrils; 2D planes of 3D spectra for full resonance assignment of P32; histograms for determining the *trans*-conformation of H31−P32 bond of hβ_2m and ΔN6 fibrils; 2D $^{15}N-^{13}C$ PAIN-CP and planes of 3D $^{15}N-^{13}C-^{13}C$ spectra of hβ_2m for the assignment of C80; histograms for identifying the redox state of C80. This material is available free of charge via the Internet at http://pubs.acs.org.

AUTHOR INFORMATION

Corresponding Author

rgg@mit.edu

Present Address

[§]Department of Chemistry, Princeton University, Princeton, NJ 08544.

Author Contributions

[⊥]Y.S. and C.J.S. have contributed equally.

Notes

The authors declare no competing financial interest.

ACKNOWLEDGMENTS

Special thanks are accorded to Geoff Platt and Theo Karamanos who have generously shared their knowledge and experiences of the sample preparation methods for hβ_2m and ΔN6. We also thank David Ruben, Christopher Turner, Jeff Bryant, and Ajay Thakkar for help with the instrumentation. We greatly appreciate Krishna Rajarathnam and Yang Shen for their insightful discussion of identifying the disulfide bond and X-Pro conformation via chemical shifts. This work was funded by NIH Grants EB003151 and EB002026 to R.G.G, MRC Grant G0900958 and Wellcome Trust Grant WT092896MA to S.E.R.

REFERENCES

(1) Chiti, F.; Dobson, C. M. *Annu. Rev. Biochem.* **2006**, *75*, 333.
(2) Eisenberg, D.; Jucker, M. *Cell* **2012**, *148*, 1188.
(3) Laganowsky, A.; Liu, C.; Sawaya, M. R.; Whitelegge, J. P.; Park, J.; Zhao, M.; Pensalfini, A.; Soriaga, A. B.; Landau, M.; Teng, P. K.; Cascio, D.; Glabe, C.; Eisenberg, D. *Science* **2012**, *335*, 1228.
(4) Sunde, M.; Blake, C. C. *Q. Rev. Biophys.* **1998**, *31*, 1.
(5) Greenwald, J.; Riek, R. *Structure* **2010**, *18*, 1244.
(6) Tycko, R.; Wickner, R. B. *Acc. Chem. Res.* **2013**, *46*, 1487.
(7) Petkova, A. T.; Leapman, R. D.; Guo, Z.; Yau, W. M.; Mattson, M. P.; Tycko, R. *Science* **2005**, *307*, 262.
(8) Baran, M. C.; Moseley, H. N.; Aramini, J. M.; Bayro, M. J.; Monleon, D.; Locke, J. Y.; Montelione, G. T. *Proteins* **2006**, *62*, 843.
(9) Paravastu, A. K.; Leapman, R. D.; Yau, W. M.; Tycko, R. *Proc. Natl. Acad. Sci. U.S.A.* **2008**, *105*, 18349.
(10) Heise, H.; Hoyer, W.; Becker, S.; Andronesi, O. C.; Riedel, D.; Baldus, M. *Proc. Natl. Acad. Sci. U.S.A.* **2005**, *102*, 15871.
(11) Comellas, G.; Lemkau, L. R.; Nieuwkoop, A. J.; Kloepper, K. D.; Ladror, D. T.; Ebisu, R.; Woods, W. S.; Lipton, A. S.; George, J. M.; Rienstra, C. M. *J. Mol. Biol.* **2011**, *411*, 881.
(12) Lv, G.; Kumar, A.; Giller, K.; Orcellet, M. L.; Riedel, D.; Fernández, C. O.; Becker, S.; Lange, A. *J. Mol. Biol.* **2012**, *420*, 99.
(13) Shewmaker, F.; Wickner, R. B.; Tycko, R. *Proc. Natl. Acad. Sci. U.S.A.* **2006**, *103*, 19754.
(14) Luckgei, N.; Schutz, A. K.; Bousset, L.; Habenstein, B.; Sourigues, Y.; Gardiennet, C.; Meier, B. H.; Melki, R.; Bockmann, A. *Angew. Chem. Int. Ed.* **2013**, *52*, 12741.
(15) Helmus, J. J.; Surewicz, K.; Nadaud, P. S.; Surewicz, W. K.; Jaroniec, C. P. *Proc. Natl. Acad. Sci. U.S.A.* **2008**, *105*, 6284.
(16) Helmus, J. J.; Surewicz, K.; Surewicz, W. K.; Jaroniec, C. P. *J. Am. Chem. Soc.* **2010**, *132*, 2393.
(17) Bayro, M. J.; Maly, T.; Birkett, N. R.; Macphee, C. E.; Dobson, C. M.; Griffin, R. G. *Biochemistry* **2010**, *49*, 7474.
(18) Jaroniec, C. P.; MacPhee, C. E.; Bajaj, V. S.; McMahon, M. T.; Dobson, C. M.; Griffin, R. G. *Proc. Natl. Acad. Sci. U.S.A.* **2004**, *101*, 711.

(19) Caporini, M. A.; Bajaj, V. S.; Veshtort, M.; Fitzpatrick, A.; MacPhee, C. E.; Vendruscolo, M.; Dobson, C. M.; Griffin, R. G. *J. Phys. Chem. B* **2010**, *114*, 13555.
(20) Fitzpatrick, A. W.; Debelouchina, G. T.; Bayro, M. J.; Clare, D. K.; Caporini, M. A.; Bajaj, V. S.; Jaroniec, C. P.; Wang, L.; Ladizhansky, V.; Muller, S. A.; MacPhee, C. E.; Waudby, C. A.; Mott, H. R.; De Simone, A.; Knowles, T. P.; Saibil, H. R.; Vendruscolo, M.; Orlova, E. V.; Griffin, R. G.; Dobson, C. M. *Proc. Natl. Acad. Sci. U.S.A.* **2013**, *110*, 5468.
(21) Bellotti, V.; Stoppini, M.; Mangione, P.; Sunde, M.; Robinson, C.; Asti, L.; Brancaccio, D.; Ferri, G. *Eur. J. Biochem.* **1998**, *258*, 61.
(22) McParland, V. J.; Kad, N. M.; Kalverda, A. P.; Brown, A.; Kirwin-Jones, P.; Hunter, M. G.; Sunde, M.; Radford, S. E. *Biochemistry* **2000**, *39*, 8735.
(23) Morgan, C. J.; Gelfand, M.; Atreya, C.; Miranker, A. D. *J. Mol. Biol.* **2001**, *309*, 339.
(24) Villanueva, J.; Hoshino, M.; Katou, H.; Kardos, J.; Hasegawa, K.; Naiki, H.; Goto, Y. *Protein Sci.* **2004**, *13*, 797.
(25) Yamamoto, S.; Yamaguchi, I.; Hasegawa, K.; Tsutsumi, S.; Goto, Y.; Gejyo, F.; Naiki, H. *J. Am. Soc. Nephrol.* **2004**, *15*, 126.
(26) Ohhashi, Y.; Kihara, M.; Naiki, H.; Goto, Y. *J. Biol. Chem.* **2005**, *280*, 32843.
(27) Myers, S. L.; Jones, S.; Jahn, T. R.; Morten, I. J.; Tennent, G. A.; Hewitt, E. W.; Radford, S. E. *Biochemistry* **2006**, *45*, 2311.
(28) Sasahara, K.; Yagi, H.; Naiki, H.; Goto, Y. *Biochemistry* **2007**, *46*, 3286.
(29) Calabrese, M. F.; Miranker, A. D. *Prion* **2009**, *3*, 1.
(30) Kad, N. M.; Thomson, N. H.; Smith, D. P.; Smith, D. A.; Radford, S. E. *J. Mol. Biol.* **2001**, *313*, 559.
(31) Eichner, T.; Kalverda, A. P.; Thompson, G. S.; Homans, S. W.; Radford, S. E. *Mol. Cell* **2011**, *41*, 161.
(32) Sarell, C. J.; Woods, L. A.; Su, Y.; Debelouchina, G. T.; Ashcroft, A. E.; Griffin, R. G.; Stockley, P. G.; Radford, S. E. *J. Biol. Chem.* **2013**, *288*, 7327.
(33) Vanderhaegen, S.; Fislage, M.; Domanska, K.; Versees, W.; Pardon, E.; Bellotti, V.; Steyaert, J. *Protein Sci.* **2013**, *22*, 1349.
(34) Jahn, T. R.; Parker, M. J.; Homans, S. W.; Radford, S. E. *Nat. Struct. Mol. Biol.* **2006**, *13*, 195.
(35) Eichner, T.; Radford, S. E. *Febs J.* **2011**, *278*, 3868.
(36) Mangione, P. P.; Esposito, G.; Relini, A.; Raimondi, S.; Porcari, R.; Giorgetti, S.; Corazza, A.; Fogolari, F.; Penco, A.; Goto, Y.; Lee, Y. H.; Yagi, H.; Cecconi, C.; Naqvi, M. M.; Gillmore, J. D.; Hawkins, P. N.; Chiti, F.; Rolandi, R.; Taylor, G. W.; Pepys, M. B.; Stoppini, M.; Bellotti, V. *J. Biol. Chem.* **2013**, *288*, 30917.
(37) Esposito, G.; Garvey, M.; Alverdi, V.; Pettirossi, F.; Corazza, A.; Fogolari, F.; Polano, M.; Mangione, P. P.; Giorgetti, S.; Stoppini, M.; Rekas, A.; Bellotti, V.; Heck, A. J.; Carver, J. A. *J. Biol. Chem.* **2013**, *288*, 17844.
(38) Becker, J. W.; Reeke, G. N. J. *Proc. Natl. Acad. Sci. U.S.A.* **1985**, *82*, 4225.
(39) Verdone, G.; Corazza, A.; Viglino, P.; Pettirossi, F.; Giorgetti, S.; Mangione, P.; Andreola, A.; Stoppini, M.; Bellotti, V.; Esposito, G. *Protein Sci.* **2002**, *11*, 487.
(40) Trinh, C. H.; Smith, D. P.; Kalverda, A. P.; Phillips, S. E.; Radford, S. E. *Proc. Natl. Acad. Sci. U.S.A.* **2002**, *99*, 9771.
(41) Rosano, C.; Zuccotti, S.; Bolognesi, M. *Biochimi. Biophys. Acta* **2005**, *1753*, 85.
(42) Iwata, K.; Matsuura, T.; Sakurai, K.; Nakagawa, A.; Goto, Y. *J. Biochem.* **2007**, *142*, 413.
(43) Smith, D. P.; Radford, S. E.; Ashcroft, A. E. *Proc. Natl. Acad. Sci. U.S.A.* **2010**, *107*, 6794.
(44) Eichner, T.; Radford, S. E. *FEBS J.* **2011**, *278*, 3868.
(45) Ami, D.; Ricagno, S.; Bolognesi, M.; Bellotti, V.; Doglia, S. M.; Natalello, A. *Biophys. J.* **2012**, *102*, 1676.
(46) Iwata, K.; Fujiwara, T.; Matsuki, Y.; Akutsu, H.; Takahashi, S.; Naiki, H.; Goto, Y. *Proc. Natl. Acad. Sci. U.S.A.* **2006**, *103*, 18119.
(47) Liu, C.; Zhao, M.; Jiang, L.; Cheng, P. N.; Park, J.; Sawaya, M. R.; Pensalfini, A.; Gou, D.; Berk, A. J.; Glabe, C. G.; Nowick, J.; Eisenberg, D. *Proc. Natl. Acad. Sci. U.S.A.* **2012**, *109*, 20913.
(48) Hoshino, M.; Katou, H.; Hagihara, Y.; Hasegawa, K.; Naiki, H.; Goto, Y. *Nat. Struct. Biol.* **2002**, *9*, 332.
(49) Chiba, T.; Hagihara, Y.; Higurashi, T.; Hasegawa, K.; Naiki, H.; Goto, Y. *J. Biol. Chem.* **2003**, *278*, 47016.
(50) Eichner, T.; Radford, S. E. *J. Mol. Biol.* **2009**, *386*, 1312.
(51) Ladner, C. L.; Chen, M.; Smith, D. P.; Platt, G. W.; Radford, S. E.; Langen, R. *J. Biol. Chem.* **2010**, *285*, 17137.
(52) Yamaguchi, K.; Katou, H.; Hoshino, M.; Hasegawa, K.; Naiki, H.; Goto, Y. *J. Mol. Biol.* **2004**, *338*, 559.
(53) Skora, L.; Becker, S.; Zweckstetter, M. *ChemBioChem* **2010**, *11*, 1829.
(54) Monti, M.; Principe, S.; Giorgetti, S.; Mangione, P.; Merlini, G.; Clark, A.; Bellotti, V.; Amoresano, A.; Pucci, P. *Protein Sci.* **2002**, *11*, 2362.
(55) Myers, S. L.; Thomson, N. H.; Radford, S. E.; Ashcroft, A. E. *Rapid Commun. Mass Spectrom.: RCM* **2006**, *20*, 1628.
(56) White, H. E.; Hodgkinson, J. L.; Jahn, T. R.; Cohen-Krausz, S.; Gosal, W. S.; Muller, S.; Orlova, E. V.; Radford, S. E.; Saibil, H. R. *J. Mol. Biol.* **2009**, *389*, 48.
(57) Debelouchina, G. T.; Platt, G. W.; Bayro, M. J.; Radford, S. E.; Griffin, R. G. *J. Am. Chem. Soc.* **2010**, *132*, 10414.
(58) Bennett, A. E.; Rienstra, C. M.; Auger, M.; Lakshmi, K. V.; Griffin, R. G. *J. Chem. Phys.* **1995**, *103*, 6951.
(59) Bennett, A. E.; Ok, J. H.; Griffin, R. G.; Vega, S. *J. Chem. Phys.* **1992**, *96*, 8624.
(60) Bennett, A. E.; Rienstra, C. M.; Griffiths, J. M.; Zhen, W. G.; Lansbury, P. T.; Griffin, R. G. *J. Chem. Phys.* **1998**, *108*, 9463.
(61) Bayro, M. J.; Maly, T.; Birkett, N. R.; Dobson, C. M.; Griffin, R. G. *Angew. Chem., Int. Ed.* **2009**, *48*, 5708.
(62) Hing, A. W.; Vega, S.; Schaefer, J. *J. Magn. Reson.* **1992**, *96*, 205.
(63) Jaroniec, C. P.; Filip, C.; Griffin, R. G. *J. Am. Chem. Soc.* **2002**, *124*, 10728.
(64) Lewandowski, J.; De Paëpe, G.; Griffin, R. G. *J. Am. Chem. Soc.* **2007**, *129*, 728.
(65) Andreas, L. B.; Eddy, M. T.; Chou, J. J.; Griffin, R. G. *J. Am. Chem. Soc.* **2012**, *134*, 7215.
(66) Daviso, E.; Eddy, M. T.; Andreas, L. B.; Griffin, R. G.; Herzfeld, J. *J. Biomol. NMR* **2013**, *55*, 257.
(67) Hing, A. W.; Vega, S.; Schaefer, J. *J. Magn. Reson., Ser. A* **1993**, *103*, 151.
(68) Delaglio, F.; Grzesiek, S.; Vuister, G. W.; Zhu, G.; Pfeifer, J.; Bax, A. *J. Biomol. NMR* **1995**, *6*, 277.
(69) Shen, Y.; Delaglio, F.; Cornilescu, G.; Bax, A. *J. Biomol. NMR* **2009**, *44*, 213.
(70) Li, Y.; Berthold, D. A.; Gennis, R. B.; Rienstra, C. M. *Protein Sci.* **2008**, *17*, 199.
(71) Franks, W. T.; Zhou, D. H.; Wylie, B. J.; Money, B. G.; Graesser, D. T.; Frericks, H. L.; Sahota, G.; Rienstra, C. M. *J. Am. Chem. Soc.* **2005**, *127*, 12291.
(72) Kloepper, K. D.; Zhou, D. H.; Li, Y.; Winter, K. A.; George, J. M.; Rienstra, C. M. *J. Biomol. NMR* **2007**, *39*, 197.
(73) Lundstrom, P.; Teilum, K.; Carstensen, T.; Bezsonova, I.; Wiesner, S.; Hansen, D. F.; Religa, T. L.; Akke, M.; Kay, L. E. *J. Biomol. NMR* **2007**, *38*, 199.
(74) Higman, V. A.; Flinders, J.; Hiller, M.; Jehle, S.; Markovic, S.; Fiedler, S.; van Rossum, B. J.; Oschkinat, H. *J. Biomol. NMR* **2009**, *44*, 245.
(75) Bayro, M. J.; Huber, M.; Ramachandran, R.; Davenport, T. C.; Meier, B. H.; Ernst, M.; Griffin, R. G. *J. Chem. Phys.* **2009**, *130*, 114506.
(76) Castellani, F.; van Rossum, B.; Diehl, A.; Schubert, M.; Rehbein, K.; Oschkinat, H. *Nature* **2002**, *420*, 98.
(77) Pauli, J.; Baldus, M.; van Rossum, B.; de Groot, H.; Oschkinat, H. *ChemBioChem* **2001**, *2*, 272.
(78) Bockmann, A.; Lange, A.; Galinier, A.; Luca, S.; Giraud, N.; Juy, M.; Heise, H.; Montserret, R.; Penin, F.; Baldus, M. *J. Biomol. NMR* **2003**, *27*, 323.

(79) Bayro, M. J.; Debelouchina, G. T.; Eddy, M. T.; Birkett, N. R.; MacPhee, C. E.; Rosay, M.; Maas, W. E.; Dobson, C. M.; Griffin, R. G. *J. Am. Chem. Soc.* **2011**, *133*, 13967.
(80) Pauli, J.; Baldus, M.; van Rossum, B.; de Groot, H.; Oschkinat, H. *ChemBioChem* **2001**, *2*, 272.
(81) Marulanda, D.; Tasayco, M. L.; McDermott, A.; Cataldi, M.; Arriaran, V.; Polenova, T. *J. Am. Chem. Soc.* **2004**, *126*, 16608.
(82) Igumenova, T. I.; Wand, A. J.; McDermott, A. E. *J. Am. Chem. Soc.* **2004**, *126*, 5323.
(83) Shi, L. C.; Ahmed, M. A. M.; Zhang, W. R.; Whited, G.; Brown, L. S.; Ladizhansky, V. *J. Mol. Biol.* **2009**, *386*, 1078.
(84) Sperling, L. J.; Berthold, D. A.; Sasser, T. L.; Jeisy-Scott, V.; Rienstra, C. M. *J. Mol. Biol.* **2010**, *399*, 268.
(85) Kameda, A.; Hoshino, M.; Higurashi, T.; Takahashi, S.; Naiki, H.; Goto, Y. *J. Mol. Biol.* **2005**, *348*, 383.
(86) Sarkar, S. K.; Torchia, D. A.; Kopple, K. D.; VanderHart, D. L. *J. Am. Chem. Soc.* **1984**, 3328.
(87) Shen, Y.; Bax, A. *J. Biomol. NMR* **2010**, *46*, 199.
(88) Huang, L.; McDermott, A. E. *Biochim. Biophys. Acta* **2008**, *1777*, 1098.
(89) Zhang, Y.; Doherty, T.; Li, J.; Lu, W.; Barinka, C.; Lubkowski, J.; Hong, M. *J. Mol. Biol.* **2010**, *397*, 408.
(90) Smith, D. P.; Radford, S. E. *Protein Sci.* **2001**, *10*, 1775.
(91) Sharma, D.; Rajarathnam, K. *J. Biomol. NMR* **2000**, *18*, 165.
(92) Long, J. R.; Sum, B. Q.; Bowen, A.; Griffin, R. G. *J. Am. Chem. Soc.* **1994**, *116*, 11950.
(93) Su, Y.; Mani, R.; Doherty, T.; Waring, A. J.; Hong, M. *J. Mol. Biol.* **2008**, *381*, 1133.
(94) Debelouchina, G. T.; Platt, G. W.; Bayro, M. J.; Radford, S. E.; Griffin, R. G. *J. Am. Chem. Soc.* **2010**, *132*, 17077.
(95) LeMaster, D. M.; Kushlan, D. M. *J. Am. Chem. Soc.* **1996**, *118*, 9255.
(96) Hong, M.; Jakes, K. *J. Biomol. NMR* **1999**, *14*, 71.
(97) Loquet, A.; Lv, G.; Giller, K.; Becker, S.; Lange, A. *J. Am. Chem. Soc.* **2011**, *133*, 4722.
(98) Bayro, M. J.; Debelouchina, G. T.; Eddy, M. T.; Birkett, N. R.; MacPhee, C. E.; Rosay, M.; Maas, W. E.; Dobson, C. M.; Griffin, R. G. *J. Am. Chem. Soc.* **2011**, *133*, 13967.
(99) Gosal, W. S.; Morten, I. J.; Hewitt, E. W.; Smith, D. A.; Thomson, N. H.; Radford, S. E. *J. Mol. Biol.* **2005**, *351*, 850.
(100) Khan, A. R.; Baker, B. M.; Ghosh, P.; Biddison, W. E.; Wiley, D. C. *J. Immunol.* **2000**, *164*, 6398.
(101) Borbulevych, O. Y.; Do, P.; Baker, B. M. *Mol. Immunol.* **2010**, *47*, 2519.
(102) Verdone, G.; Corazza, A.; Viglino, P.; Pettirossi, F.; Giorgetti, S.; Mangione, P.; Andreola, A.; Stoppini, M.; Bellotti, V.; Esposito, G. *Protein Sci.* **2002**, *11*, 487.
(103) Ricagno, S.; Colombo, M.; de Rosa, M.; Sangiovanni, E.; Giorgetti, S.; Raimondi, S.; Bellotti, V.; Bolognesi, M. *Biochem. Biophys. Res. Commun.* **2008**, *377*, 146.
(104) Hodkinson, J. P.; Jahn, T. R.; Radford, S. E.; Ashcroft, A. E. *J. Am. Soc. Mass Spectrom.* **2009**, *20*, 278.
(105) Rennella, E.; Corazza, A.; Fogolari, F.; Viglino, P.; Giorgetti, S.; Stoppini, M.; Bellotti, V.; Esposito, G. *Biophys. J.* **2009**, *96*, 169.
(106) Colombo, M.; Ricagno, S.; Barbiroli, A.; Santambrogio, C.; Giorgetti, S.; Raimondi, S.; Bonomi, F.; Grandori, R.; Bellotti, V.; Bolognesi, M. *J. Biochem.* **2011**, *150*, 39.
(107) Platt, G. W.; Routledge, K. E.; Homans, S. W.; Radford, S. E. *J. Mol. Biol.* **2008**, *378*, 251.
(108) Stoppini, M.; Bellotti, V.; Mangione, P.; Merlini, G.; Ferri, G. *Eur. J. Biochem.* **1997**, *249*, 21.
(109) Ohhashi, Y.; Hagihara, Y.; Kozhukh, G.; Hoshino, M.; Hasegawa, K.; Yamaguchi, I.; Naiki, H.; Goto, Y. *J. Biochem.* **2002**, *131*, 45.
(110) Hong, D. P.; Gozu, M.; Hasegawa, K.; Naiki, H.; Goto, Y. *J. Biol. Chem.* **2002**, *277*, 21554.
(111) Katou, H.; Kanno, T.; Hoshino, M.; Hagihara, Y.; Tanaka, H.; Kawai, T.; Hasegawa, K.; Naiki, H.; Goto, Y. *Protein Sci.* **2002**, *11*, 2218.
(112) Jahn, T. R.; Makin, O. S.; Morris, K. L.; Marshall, K. E.; Tian, P.; Sikorski, P.; Serpell, L. C. *J. Mol. Biol.* **2010**, *395*, 717.
(113) Griffin, R. G. *Nature* **2010**, *468*, 381.
(114) Ni, Q. Z.; Daviso, E.; Can, T. V.; Markhasin, E.; Jawla, S. K.; Swager, T. M.; Temkin, R. J.; Herzfeld, J.; Griffin, R. G. *Acc. Chem. Res.* **2013**, *46*, 1933.
(115) Rossini, A. J.; Zagdoun, A.; Lelli, M.; Lesage, A.; Coperet, C.; Emsley, L. *Acc. Chem. Res.* **2013**, *46*, 1942.